RESEARCH Open Access

CircPRKCA facilitates esophageal squamous cell carcinoma metastasis via m5C-dependent CSF2 mRNA stabilization

Lixia Wu^{1,2†}, Lina Gu^{1,2†}, Yang zheng^{1,2}, Jingjing Liu^{1,2}, Zishuan Wei^{1,2}, Fei Liu^{1,2}, Jiali Li^{1,2}, Lingjiao Meng^{1,2}, Yang Sang³, Meixiang Sang⁴, Lianmei Zhao^{1,2*} and Baoen Shan^{1,2*}

Abstract

Background Esophageal squamous cell carcinoma (ESCC) is a serious invasive malignancy with an ambiguous etiology. Evidence indicates that circular RNA (circRNA) is significantly involved in the regulatory processes associated with cancer development. Nevertheless, the specific molecular mechanisms through which circRNA facilitates the progression of ESCC are still largely undefined.

Methods Here, we identified that the expression of hsa_circ_0007580 (designated circPRKCA) was markedly elevated in ESCC. Fluorescence in situ hybridization (FISH) was conducted to verify the expression, intracellular localization, and potential prognostic value of circPRKCA based on the tissue microarray. Gain- and loss-of-function assays were employed to investigate the effects of circPRKCA both in vitro and in vivo. RNA pull-down and mass spectrometry (MS) were performed to identify the proteins bound to circPRKCA. mRNA sequencing was conducted to screen the downstream target genes of circPRKCA. Furthermore, immunoprecipitation and methylated RNA immunoprecipitation (MeRIP) analysis were used to explore the regulatory mechanisms.

Results We found that circPRKCA exhibited significant upregulation in ESCC tissues and correlated with unfavorable prognostic outcomes. Biological function experiments further confirmed that circPRKCA enhances the capabilities of migration, invasion, and angiogenesis in ESCC. Mechanistically, circPRKCA engages in interaction with Y-box binding protein 1 (YBX1) within the cytoplasmic milieu, consequently preventing the ubiquitination-mediated degradation of YBX1. Increased concentrations of YBX1 increase the stability of granulocyte–macrophage colony-stimulating factor (CSF2) mRNA in a 5-methylcytosine (m5C)-dependent manner. This process facilitates metastasis in ESCC.

Conclusion In this research, we identified a correlation between circPRKCA and unfavorable prognoses in patients with ESCC. It is instrumental in the metastatic progression of ESCC via the YBX1/CSF2 signaling pathway. Consequently, targeting circPRKCA may represent a promising therapeutic strategy for ESCC.

Keywords ESCC, CircPRKCA, YBX1, CSF2, Prognosis

[†]Lixia Wu and Lina Gu have contributed equally to this work.

*Correspondence: Lianmei Zhao lianmei555@hebmu.edu.cn Baoen Shan 462000595@hebmu.edu.cn Full list of author information is available at the end of the article



Background

Esophageal cancer (EC) is one of the most common malignant tumors globally [1], with esophageal squamous cell carcinoma (ESCC) being the predominant pathological type in China and ranking as the fifth leading cause of cancer-related mortality [2]. Due to its highly invasive and metastatic nature, the five-year survival rate for advanced-stage patients is less than 15% [3]. Therefore, investigating the mechanisms that promote ESCC metastasis is of critical importance.

Circular RNAs (circRNAs) have been identified as regulators of cancer progression. CircRNAs are covalently closed-loop structures formed through back-splicing or exon skipping of precursor mRNAs [4]. Lacking 5' caps and 3' poly(A) tails, circRNAs exhibit resistance to exonuclease degradation and enhanced stability. These characteristics make circRNAs viable candidates as detectable biomarkers. Studies have demonstrated that circRNAs exhibit aberrant expression patterns in various cancers. Such dysregulation holds the potential to modulate tumor progression by functioning as miRNA sponges, protein scaffolds, or even encoding polypeptides [5]. For instance, circHIPK3 has been characterized as a competing endogenous RNA (ceRNA) that sponging miR-637, thereby regulating FASN expression and fatty acid metabolism in ESCC cells [6]. Similarly, the upregulation of hsa circ 0001165 has been shown to modulate the miR-381-3p/TNS3 axis, driving aggressive phenotypes in ESCC [7]. While the role of circRNAs as miRNA sponges has been extensively explored in ESCC, emerging evidence highlights the significance of circRNA interactions with RNA-binding proteins (RBPs) in promoting tumor progression [8, 9]. Nevertheless, the precise molecular mechanisms underlying these circRNA-RBP interactions in ESCC remain poorly understood and warrant further investigation.

To find the key driver circRNAs in ESCC tissues, our research team previously conducted high-throughput sequencing analysis on five pairs of ESCC tissues and matched adjacent non-cancerous tissues [10]. Among the top 50 differentially expressed circR-NAs, we focused on a highly enriched circRNA, hsa_ circ_0007580, due to its parent gene PRKCA being recognized as an oncogene [11]. However, the specific regulatory mechanisms and functional pathways of circPRKCA in ESCC remain unclear. Y-box binding protein 1(YBX1), a multifunctional DNA- and RNAbinding protein, is frequently upregulated in various cancers and has been strongly implicated in cancer metastasis [12]. It plays a pivotal role in regulating mRNA stability, suppressing translational repression, and modulating transcriptional activity, all of which contribute to the metastatic progression of cancer [13, 14]. Additionally, granulocyte-macrophage colony-stimulating factor (CSF2), a tumor-derived growth factor, is widely recognized for its role in promoting angiogenesis. Furthermore, CSF2 drives epithelial-mesenchymal transition (EMT) and enhances immune checkpoint expression, thereby facilitating the malignant progression of multiple tumor types [15–17].

In our study, we identified a correlation between circPRKCA and unfavorable prognoses in patients with ESCC. Mechanistically, circPRKCA interacts with YBX1, preventing its ubiquitination-mediated degradation. The increased YBX1 stabilizes CSF2 mRNA in a 5-methylcytosine (m5C)-dependent manner, facilitating ESCC metastasis. Our findings reveal a novel regulatory mechanism, highlighting the potential of circPRKCA as a biomarker for assessing metastatic risk in ESCC patients and as a promising target for therapeutic intervention.

Materials and methods

Cell culture and transfection

The human ESCC cell lines used in this study are all available in our laboratory, including TE1, KYSE30, KYSE410, and KYSE150 (Procell, Wuhan). No evidence of mycoplasma contamination was observed, as verified by the Mycoplasma detection test kit (Seven, Beijing). The principles of cell line selection are as follows: TE1 and KYSE30 with relatively high expression were chosen to verify the cyclization characteristics of circPRKCA. To investigate the subcellular localization of circPRKCA and the specific mechanisms that promote the progression of ESCC, KYSE30 with relatively high expression of circPRKCA and KYSE150 with relatively low expression of circPRKCA were selected for dual verification. To model the tumor-promoting process mediated by circPRKCA in vivo, KYSE150 with relatively low expression of circPRKCA was utilized to overexpress circPRKCA for the animal experiments. Cells were cultured in RPMI 1640 medium enriched with 10% fetal bovine serum (FBS), along with 100 U/ml penicillin and 100 μg/ml streptomycin, or in F-12 medium (GIBCO, USA). The cultures were sustained in a humidified atmosphere containing 5% CO2 at a temperature of 37 °C.

For transfection experiments, siRNA (RiboBio, Guangzhou) or plasmid DNA (Geneseed, Guangzhou) was used. ESCC cells (1×10^6) were seeded in 6-well plates and transfected with siRNA using HiperFect or with plasmid DNA using PolyFect transfection reagents (Qiagen GmbH), according to the manufacturer's instructions. After 6 h of transfection, the medium was replaced with complete growth medium, and cells were harvested 48 h post-transfection for further analysis.

Tissue microarray sample

The clinical tissue microarray sample HEsoS180Su11 (catalog no. YB M-05-02; approval no. SHYJS-CP-2004003) used in this study was purchased from Shanghai Outdo Biotech Company. This microarray included 108 ESCC specimens and 64 adjacent non-tumor tissues. Detailed clinicopathological characteristics and survival outcomes were documented for all patients. Written informed consent was obtained from each participant prior to inclusion in the study. The research protocol was approved by the Institutional Review Committee of Shanghai Outdo Biotechnology Co., Ltd.

Genomic DNA (gDNA) and RNA extraction, reverse transcription-quantitative polymerase chain reaction, and agarose gel electrophoresis

Genomic DNA was extracted using a gDNA extraction kit (TANGEN, China), and total RNA was isolated using the Trizol method (Invitrogen, USA). The purity of DNA and RNA was assessed spectrophotometrically, with acceptable ranges as follows: for DNA, A260/A280: 1.7–1.9 and A260/A230: 2.0–2.2; for RNA, A260/A280: 1.8–2.0 and A260/A230: 2.0–2.2. Complementary DNA (cDNA) was synthesized using the GoScript Reverse

Transcription System (Promega, USA). Quantitative PCR (qPCR) was performed using SYBR Green qPCR Master Mix II (Seven, Beijing), with primers listed in Table 1. U6 and GAPDH were used as internal controls for circRNA and mRNA, respectively. The qPCR reaction program consisted of an initial denaturation at 95 °C for 5 min, followed by 40 cycles of denaturation at 95 °C for 15 s, annealing at 60 °C for 30 s, and extension at 72 °C for 30 s, with a final extension at 72 °C for 10 min. Gene expression levels were quantified using the $2^{-\Delta\Delta Ct}$ method [18]. For PCR, the reaction conditions included pre-denaturation at 95 °C for 5 min, followed by 35 cycles of denaturation at 95 °C for 45 s, annealing at 60 °C for 45 s, and extension at 72 °C for 60 s, with a final extension at 72 °C for 10 min. PCR products were separated by 2% agarose gel electrophoresis and visualized using Safe Green (Monad, China) under 120 V for 60 min.

Nuclear and cytoplasmic fractionation

Nuclear and cytoplasmic fractions were isolated using the extraction kit specified by Pierce (Thermo Fisher Scientific, Inc.). Briefly, cells were lysed using a cell fractionation buffer and incubated on ice for 10 min. The lysate was then centrifuged at $500 \times g$ for 3 min. The

Table 1 List of primers sequences

Experiment types	Gene	Primers	Product size (bp)		
RT-PCR and RT-qPCR	circPRKCA Divergent primer	F:5'—GTGCAAGGAACACATGATGG—3' R:5'—ACTCGGTCAAGGTTGTTGGA—3'	156		
	circPRKCA Convergent primers	F:5'—AAGGCTTCCAGTGCCAAGTT—3' R:5'—CTCCTGGGGTCATCAGTGTC—3	112		
	YBX1	F:5'—GGACAAGAAGGTCATCGCAAC—3' R:5'—TCTCCATCTCCTACACTGCGA—3'	171		
	CSF2	F:5'—ATCCCCTTTGACTGCTGGGA—3' R:5'—TTGGTCCCTCCAAGATGACC—3	126		
	GAPDH	F:5'—CGCTGAGTACGTCGTGGAGTC—3' R:5'—GCTGATGATCTTGAGGCTGTTGTC—3'	172		
	U6	F:5'—CTCGCTTCGGCAGCACA—3' R:5'—AACGCTTCACGAATTTGCGT—3'	92		
Transfection	Target sequence circPRKCA-si1	5'—CCCAGAGAAAGCCAAACTT—3'			
	Target sequence circPRKCA-si2-	5'—CAGAGAAAGCCAAACTTGG—3'			
	Target sequence circPRKCA-si3	5'—CCAGAGAAAGCCAAACTTG—3'			
	YBX1-si1	F:5'—CAAGGAAGAUGUAUUUGUATT—3' R:5'—UACAAAUACAUCUUCCUUGTT—3'			
	YBX1-si2	F: 5'—CGGCAAUGAAGAAGAUAAATT –3' R:5'—UUUAUCUUCAUUGCCGTT-3'			
	YBX1-si3-	F: 5'—GGCGAAGGUUCCCACCUUATT—3' R:5'—UAAGGUGGGAACCUUCGCCTT—3'			
FISH RNA pull-down	circPRKCA probe	5'—/5bio/-GCAGGGCCAA GTTTGGCTTT CTCTGGGGCG ATATAATCTG-3'			

supernatant, representing the cytoplasmic fraction, was carefully collected, while the pellet was washed with lysis buffer to obtain the nuclear fraction. Subsequently, 500 μl of lysis binding solution was added to each fraction, followed by the addition of an equal volume of absolute ethanol. The mixtures were thoroughly vortexed to ensure homogeneity. Each mixture was then transferred to a filtration column, and the filtrate was discarded. The columns were washed twice with wash buffer and centrifuged at 12,000 \times g for 30 s. Finally, RNA was eluted using 50 μl of elution buffer. The isolated RNA was quantified by RT-qPCR for further analysis.

Actinomycin D assay

All cells were pre-plated into culture plates. To evaluate the half-life of circPRKCA, actinomycin D (AdooQ Bioscience, USA) was added to the cell cultures at a concentration of 2 μ g/ml, and samples were collected at 0, 4-, 8-, 12-, and 24 h post-treatment. For the CSF2 half-life assay, due to its relatively short half-life, samples were collected at 0, 20, 40, and 60 min after the addition of 2 μ g/ml actinomycin D. Following treatment, total RNA was extracted using the Trizol method (Invitrogen, USA), and RNA stability was assessed by RT-qPCR.

Fluorescence in situ hybridization (FISH)

FISH was performed to determine the subcellular localization of circPRKCA in ESCC cell lines (KYSE30 and KYSE150) and to analyze circPRKCA expression in ESCC tissue microarrays (HEsoS180Su11, catalog no. YB M-05-02, approval no. SHYJS-CP-2004003, Shanghai Outdo Biotech Company). ESCC cells were seeded onto glass coverslips in 12-well plates and cultured for 24 h. Cells were fixed with 4% paraformaldehyde for 20 min and permeabilized with 0.1% Triton X-100 on ice for 5 min. To prevent non-specific binding, cells were prehybridized with a 100×blocking solution (150 µl PBST, 3 μl sheep serum, and 3.3 μl 30% BSA). Hybridization was performed overnight at 37 °C using a circPRKCA probe (Geneseed, Guangzhou). For ESCC tissue sections, dewaxing was performed, followed by incubation with Protease K at 37 °C for 10 min. Pre-hybridization and probe hybridization were subsequently carried out overnight. The next day, circPRKCA was labeled using Cy5-Streptavidin Conjugate (ZyMAX™ Grade, Invitrogen), and nuclei were counterstained with DAPI. Fluorescence signals were visualized and captured using laser confocal microscopy (LSM 900, Zeiss, Germany). Two experienced pathologists, trained on standardized scoring criteria, independently analyzed the FISH staining. Any discrepancies between their evaluations were resolved through discussion and re-evaluation by a third pathologist to ensure consensus. All pathologists were blinded to the patient clinical outcomes.

Five fields of view were randomly selected for each tissue section to assess the staining intensity of positive cells. The evaluation criteria were as follows [19]: (1) Most cells exhibited no or only weak red fluorescence, resulting in a score of 0; (2) Most cells displayed low intensity, or more than 50% of cells showed moderate intensity, resulting in a score of 1; (3) Most cells with medium and high intensity received a score of 2. A score of ≤ 1 indicates low expression, while a score of > 1 indicates high expression.

Cell counting kit-8 (CCK-8) assay and colony formation assays

For the CCK-8 assay, ESCC cells (4×10^3) were seeded into 96-well plates. The OD450 value was measured at 0, 24, 48, 72, and 96 h using the Cell Counting Kit-8 (Med Chem Express, USA). For colony formation assays, 1000 ESCC cells were cultured for 1 to 2 weeks. Colonies were fixed with 4% paraformaldehyde and stained with crystal violet. A colony was considered viable if it contained \geq 50 cells.

Scratch healing assay

ESCC cells were seeded at a density of 5×10^5 cells/mL per well in 6-well plates. When the cells reached approximately 80% confluence, vertical scratches were made in each well using a sterile 10 μ L pipette tip. The initial scratch width was recorded at 0 h. After 24 h of incubation in serum-free medium, the scratch width was measured again. The scratch healing rate was calculated using the following formula: [(scratch width at 0 h–scratch width at 24 h)/(scratch width at 0 h)] \times 100%.

Transwell migration and matrigel invasion assays

Transwell chambers (BD Biosciences, USA) without or with matrigel coating were used to evaluate the migration and invasion capabilities of ESCC cells. ESCC cells (4×10^4) were evenly distributed in the upper chamber, which contained 200 μ L of serum-free medium, while 600 μ L of complete medium was added to the lower chamber. After 24 to 48 h of incubation, the cells were fixed with 4% paraformaldehyde and stained with crystal violet. Images were captured using an inverted phase-contrast microscope (DFC295, Leica, Buffalo Grove, USA) for further analysis.

Tube formation assay

A tube formation assay was performed to evaluate the ability of circPRKCA to promote angiogenesis. Briefly, matrigel (Corning, USA) was added to a 96-well plate and incubated at 37 °C for 2 h to solidify. Human umbilical

vein endothelial cells (HUVECs) were seeded at a density of 1.5×10^4 cells per well in 100 μ L of conditioned medium and cultured for 4 to 12 h. Tube formation was visualized and captured using an inverted phase-contrast microscope (DFC295, Leica, Buffalo Grove, USA). Images were analyzed using ImageJ software to quantify the angiogenic capacity.

Enzyme-linked immunosorbent assay (ELISA)

Cell culture supernatants were collected and analyzed for cytokine production using a Human CSF2 ELISA kit (Proteintech, Wuhan, China) according to the manufacturer's protocol. Briefly, 100 µL of standards and samples were added to a 96-well plate and incubated at 37 °C for 2 h. The wells were washed four times with 400 μL of wash buffer. Subsequently, 100 µL of CSF2 detection antibody was added to each well and incubated at 37 °C for 1 h, followed by another four washes. Next, 100 μL of enzyme-linked streptavidin secondary antibody was added and incubated for 40 min. After four additional washes, 100 µL of TMB substrate solution was added and incubated for 20 min. The reaction was terminated by adding 100 µL of stop solution. Absorbance was measured at 450 nm, and the CSF2 concentration in the samples was determined based on the standard curve.

RNA pull-down assays

To identify proteins interacting with circPRKCA in ESCC cell lines (KYSE30 and KYSE150), a ChIRP (Chromatin Isolation by RNA Purification) probe targeting the cyclization junction of circPRKCA was synthesized by Ribo-Bio (Guangzhou, China). Cell lysates (1×10^7 cells) were incubated with 50 pmol of biotin-labeled circPRKCA probe or a control probe for 2 h. The resulting complexes were then incubated with 50 μ L of streptavidin C1 magnetic beads (Invitrogen; Thermo Fisher Scientific) for 1 h. After three washes with buffer, the bound proteins were eluted and subjected to mass spectrometry (MS) or Western blot analysis.

Cycloheximide (CHX) chase assay and MG132 assay

To evaluate the stability of the YBX1 protein, CHX and MG132 assays were performed. ESCC cells were seeded in 6-well plates and transfected for 48 h. For the CHX chase assay, cells were treated with 40 $\mu g/mL$ CHX for 0, 3, 6, and 9 h. For the MG132 assay, cells were treated with either DMSO or 20 μM MG132 for 6 h. After treatment, cells were harvested for protein extraction, and YBX1 protein levels were analyzed by Western blot.

Co-immunoprecipitation(Co-IP)

Co-IP was performed to evaluate the regulatory role of ubiquitination on YBX1. ESCC cells were treated with MG132 for 6 h, the cells were harvested and lysed in Co-IP buffer supplemented with proteasome inhibitors. The lysates were incubated overnight with either IgG (2 μ g antibody for 2 mg protein, 30,000-0-AP, Proteintech, Wuhan, China) or IP antibodies. The following day, 30 μ L of agarose beads were added to the lysate-antibody complex and gently mixed at 4 °C for 1 h. After washing the beads three times with buffer, SDS sample buffer was added to the beads. The mixture was then heated at 100 °C for 5 min and subjected to Western blot analysis.

Western blot analysis

Total protein was extracted using RIPA lysis buffer supplemented with protease inhibitors. Protein concentrations were quantified using the BCA assay. Proteins were separated by 10% SDS-PAGE and transferred to a PVDF membrane (Merck Millipore, Germany). The membrane was blocked with 5% bovine serum albumin (BSA) for 1 h and then incubated with the primary antibody at 4 °C overnight. After three washes with TBST, the membrane was incubated with horseradish peroxidase (HRP)-conjugated Affinipure Goat Anti-Rabbit IgG (H+L) antibody (1:10,000) or HRP-conjugated IgG Fraction Monoclonal Mouse Anti-Rabbit IgG, Light Chain Specific (1:6,000) for 1 h at 37 °C. Following additional washes with TBST, immunoreactive signals were detected using electrochemiluminescence (ECL) (Thermo Scientific, USA). The grayscale values of the protein bands were analyzed using ImageJ software.

In vivo tumorigenesis assays

Animal experiments were conducted in compliance with established scientific and ethical standards. BALB/c nude mice were randomly assigned to groups using a random number table, with strict exclusion criteria applied. Mice exhibiting significant health issues, such as infectious diseases, severe injuries, physical deformities, or unexpected mortality during the experiment, were systematically excluded. During the data collection process, the researchers were blinded to the group assignments, but they were aware of the groups during the statistical analysis phase. The study protocol was approved by the Animal Care and Use Committee of the Fourth Affiliated Hospital of Hebei Medical University (Shijiazhuang, China; Approval No. IACUC-4th Hos Hebmu-2023223).

Male BALB/c nude mice (4–5 weeks old) were purchased from Beijing Huafukang Biotechnology Co., Ltd. The mice were randomly divided into two groups (n=4 per group) and injected via the tail vein with 1×10^6 KYSE150 cells transfected with either pLC5 or circPRKCA. Mice were monitored regularly for eight weeks post-injection. After eight weeks of cell injection, mice were euthanized by cervical dislocation, and their

lungs were excised and fixed in formalin. The number of pulmonary metastatic nodules was quantified to assess metastatic potential.

mRNA sequencing

To identify target genes regulated by circPRKCA, total RNA was extracted from ESCC cells transfected with si-NC or si-circPRKCA. Mycoplasma contamination was excluded using a Mycoplasma Detection Kit (Seven, China). Three biological replicates were prepared for each condition. RNA quality assessment and transcriptome sequencing were performed by Hangzhou LC-Biotechnology Co., Ltd. Differential expression analysis was conducted using reads count data as input. A p-value calculation model based on the negative binomial distribution was applied for statistical analysis. DESeq2 was used for biological replicate analysis, while edgeR was employed for multi-group comparisons. The fold change (FC) was calculated as the ratio of the mean expression in the experimental group to the mean expression in the control group. Differentially expressed genes were identified using thresholds of $|\log 2FC| \ge 1$ and p < 0.05.

RNA Immunoprecipitation (RIP) assay

To investigate the interaction between YBX1 and CSF2, RIP was performed using a RIP kit (Geneseed, Guangzhou, China) according to the manufacturer's protocol. Briefly, 2×10^7 cells were resuspended in lysis buffer and centrifuged. The lysates were incubated overnight at 4 °C with antibody-conjugated magnetic beads specific to YBX1 or IgG (5 μ g antibody, 30,000-0-AP, Proteintech, Wuhan, China). RNA was extracted from the immunoprecipitated complexes, and the relative expression levels were quantified by RT-qPCR.

Immunohistochemical(IHC) analysis

IHC was used to assess protein expression in tumor tissues. Tumor sections were deparaffinized, and endogenous peroxidase activity was quenched using 3% hydrogen peroxide. The slides were incubated with primary antibodies against YBX1, CSF2, CD31, and CD34 at 4 °C for 12 h, followed by incubation with HRP-conjugated secondary antibodies. Antigen detection was carried out using diaminobenzidine (DAB), and nuclei were counterstained with hematoxylin. IHC results were evaluated in a blinded manner, consistent with the FISH assay scoring approach. Staining intensity and extent were scored according to previously established criteria [20]. Samples were classified as negative (0), weak (1–2), moderate (3), or strong (4–6) based on the combined scores.

Antibodies

The antibodies used in this study were sourced from commercial suppliers as follows: anti-YBX1 for Western blot (1:5000 dilution, 20,339-1-AP, Proteintech, Wuhan, China); anti-β-actin for Western blot (1:1000 dilution, ab8227, Abcam, Massachusetts, USA); anti-Ub polyclonal antibody for Western blot (1:5000 dilution, 10,201-2-AP, Proteintech, Wuhan, China); anti-YBX1 for IHC (1:1000 dilution, 20,339-1-AP, Proteintech, Wuhan, China); anti-CSF2 for IHC (1:500 dilution, 17,762-1-AP, Proteintech, Wuhan, China); anti-CD31 for IHC (1:200 dilution, 11,265-1-AP, Proteintech, Wuhan, China); anti-CD34 for IHC (1:200 dilution, 14,486-1-AP, Proteintech, Wuhan, China); anti-YBX1 for FISH-IF (1:200, 20,339-1-AP, Proteintech, Wuhan, China); anti-YBX1 for RIP (5 µg anti-20,339-1-AP, Proteintech, Wuhan, China); anti-m5C for MeRIP (5 µg antibody, ab10805, Abcam, Massachusetts, USA); anti-YBX1 for Co-IP (2 µg antibody, 20,339-1-AP, Proteintech, Wuhan, China); anti-Ub for Co-IP (2 μg antibody, 10,201-2-AP, Proteintech, Wuhan, China).

Statistical analysis

Statistical analysis was performed using SPSS version 19.0 (IBM Corp.) and GraphPad Prism 9.0 (GraphPad Software). Group means were compared using Student's t-test, and the chi-square test was utilized to analyze the clinicopathological data across the groups. Survival curves were generated using the Kaplan–Meier method. Both univariate and multivariate analyses were conducted to assess the prognostic significance of various factors. *p<0.05, **p<0.01, ***p<0.001 were considered indicative of a statistically significant difference.

Results

Verification of characteristics of circPRKCA in ESCC cells

CircPRKCA was cyclized with exons 9–13 of PRKCA, resulting in a length of 606 nt. We designed specific divergent primers to amplify the cyclization splicing site of circPRKCA and confirmed its existence through Sanger sequencing (Fig. 1A). The sequencing results align with the annotations in the circBase database (http://www.circbase.org/). Agarose gel electrophoresis demonstrated that the divergent priming of circPRKCA could be amplified in cDNA but not in gDNA (Fig. 1B). Additionally, experiments using actinomycin D revealed that circPRKCA exhibited greater stability than its linear transcript (Fig. 1C, D). Furthermore, FISH assays, along with nuclear and cytoplasmic separation analyses, indicated

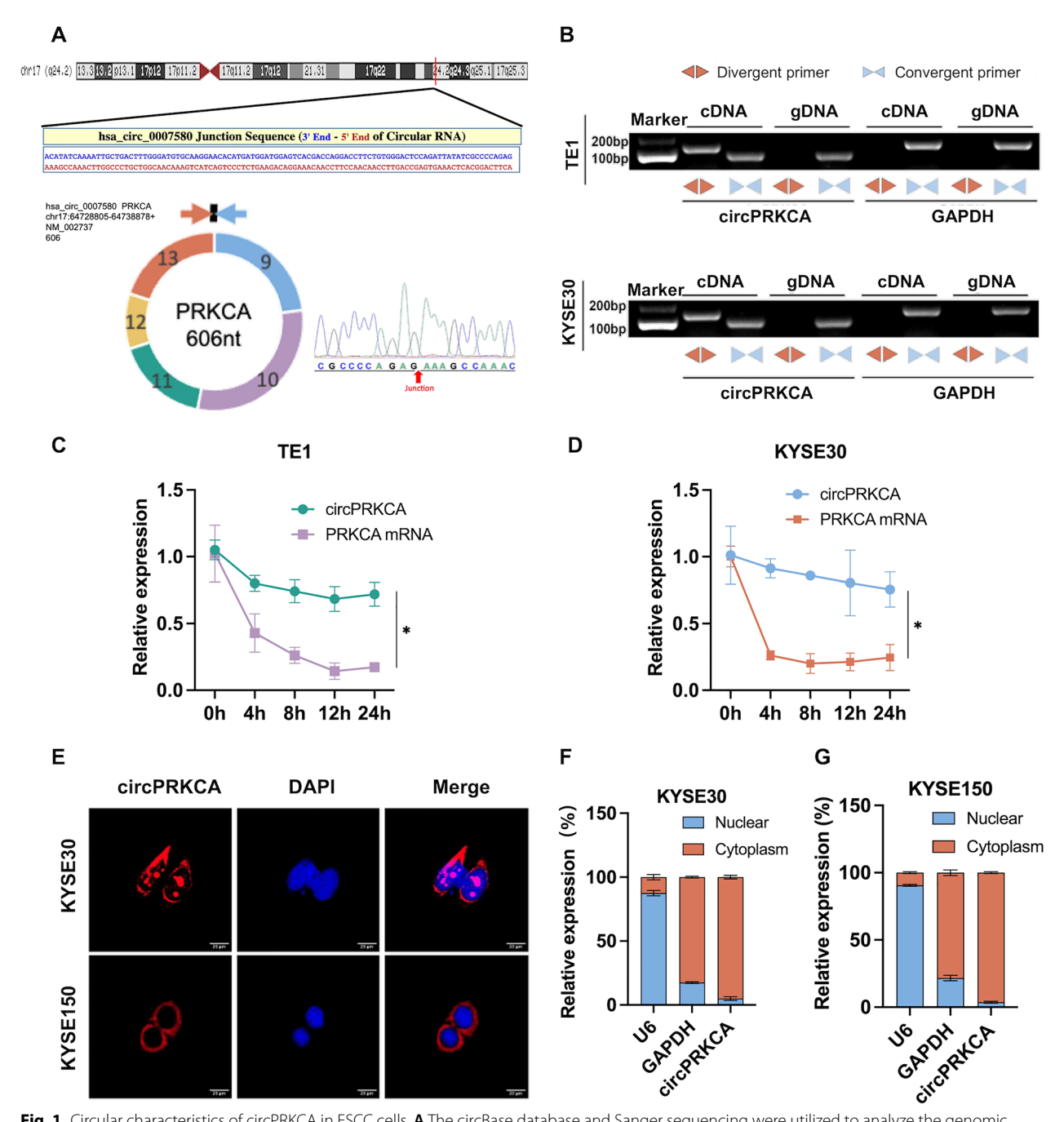


Fig. 1 Circular characteristics of circPRKCA in ESCC cells. **A** The circBase database and Sanger sequencing were utilized to analyze the genomic structure and back-splicing sites of circPRKCA. **B** RT-PCR confirmed the presence of circPRKCA. **C**, **D** RT-qPCR was employed to assess the stability of circPRKCA and PRKCA mRNA at specified time points. **E** The subcellular localization of circPRKCA detected by FISH. **F**, **G** The subcellular distribution of circPRKCA was assessed through nucleus-cytoplasmic separation. *p < 0.05, ***p < 0.01, ****p < 0.001

that circPRKCA was predominantly localized in the cytoplasm (Fig. 1E–G).

CircPRKCA is highly expressed in ESCC tissues and is associated with a poor prognosis

The expression of circPRKCA in 108 ESCC tissues and 64 corresponding adjacent tissues was analyzed using RNA FISH based on tissue microarray technology. The

results showed that circPRKCA expression was significantly higher in ESCC tissues than in adjacent tissues. (Fig. 2A, B). Analysis of the relationship between circPRKCA expression and clinicopathological characteristics in ESCC patients revealed that circPRKCA levels were higher in those with lymph node metastasis and advanced clinical stages (Fig. 2C, D and Table 2). Kaplan-Meier analysis indicates that patients with ESCC exhibiting elevated levels of circPRKCA expression experience a diminished overall survival (Fig. 2E). Furthermore, Cox regression analysis confirmed that high circPRKCA expression was an independent prognostic risk factor for ESCC patients (Fig. 2F and Table 3). The results indicate that circPRKCA is significantly overexpressed in ESCC tissues and correlates with a poor prognosis for patients. This prompted us to validate this conclusion through functional cell biology experiments.

High expression of circPRKCA is associated with ESCC metastasis in vitro and in vivo

RT-qPCR was used to verify the expression of circPRKCA in four ESCC cell lines. The results indicated that circPRKCA expression was relatively high in TE1 and KYSE30 cells, while it was comparatively low in KYSE410 and KYSE150 cells (Fig. S1A). We designed specific siR-NAs targeting the cyclization splicing site to effectively reduce circPRKCA expression in TE1 and KYSE30 cells (Fig. S1B). Additionally, a circPRKCA overexpression plasmid was successfully constructed to elevate the expression of circPRKCA without affecting the linear expression of PRKCA mRNA in KYSE410 and KYSE150 cells, compared to the pLC5 vector (Fig. S1C). Next, both loss- and gain- of-function approaches were utilized to explore the biological function of circPRKCA. CCK-8 and colony formation assays showed that circPRKCA did not effectively affect the proliferation of ESCC cells (Fig. S1D-I). Scratch healing, transwell migration and martigel invasion assays revealed that circPRKCA knowdown significantly inhibited the migration and invasion capabilities of TE1 and KYSE30 cells (Figs. 3A, C and S2A, S2C). Conversely, circPRKCA overexpression exhibited opposing effects in KYSE410 and KYSE150 cells (Figs. 3B, D and S2B, S2D). To evaluate the angiogenic potential of circPRKCA, tube formation assays were conducted. The result showed that circPRKCA inhibited the angiogenic characteristics of HUVEC cells cultured with the conditioned medium from TE1 and KYSE30 cells transfected with si1-circPRCKA and si3-circPRKCA (Figs. 3E and S2E). In contrast, circPRKCA significantly enhanced the angiogenic capacity of HUVECs treated with conditioned medium from KYSE410 and KYSE150 cells transfected with the circPRKCA overexpression vector (Figs. 3F and S2F). These results suggest that circPRKCA substantially augments metastasis-related characteristics in ESCC cells.

To further investigated the function of circPRKCA in facilitating the progression of ESCC in vivo. Initially, we transfected KYSE150 cells with pLC5 and circPRKCA vectors, followed by resistance screening using purinomycin (2 µg/ml) to establish stable transfected cell lines. A sustained increase in the migratory phenotype was observed (Fig. S2G, S2H). We then constructed a lung metastasis model by injecting BALB/c mice via the tail vein with KYSE150 cells that stably overexpressed either the circPRKCA vector or the pLC5 vector (Fig. 3G). The mice were monitored regularly and euthanized after 8 weeks. The preserved lung tissue containing metastatic nodules was stained with hematoxylin and eosin (H&E) (Fig. 3H). These results indicated that the number of pulmonary metastatic nodules in the circPRKCA group was significantly higher than that in the pLC5 group (Fig. 3I), suggesting that circPRKCA functions as a carcinogenic factor in ESCC.

CircPRKCA binds to the YBX1 protein to promote metastasis in ESCC

Next, we investigated the molecular mechanism by which circPRKCA promotes metastasis in ESCC cells. RNA pull-down, silver staining and MS were conducted to enrich and identify for proteins that bind to circPRKCA (Figs. 4A and S3A). Notably, AGO2, a protein known to be associated with miRNA sponging mechanisms, was absent from the MS results. This suggests that circPRKCA may not function as a miRNA sponge. Furthermore, the circRNADb dataset (http://reprod.njmu.edu.cn/cgi-bin/circRNADb.php) did not predict an open reading frame (ORF) or an internal ribosome entry site (IRES) for circPRKCA, indicating that it may be a non-coding

(See figure on next page.)

Fig. 2 High expression of circPRKCA in ESCC tissues and its impact on the prognosis of ESCC patients. **A** Representative images of circPRKCA expression analyzed using FISH on tissue microarrays. **B** CircPRKCA expression ratio in 108 ESCC tissues compared to 64 adjacent tissues. **C** Distributions of clinical stages were analyzed according to circPRKCA expression level in 108 ESCC tissues. **D** Rates of lymph node metastasis were analyzed based on the expression levels of circPRKCA in 108 ESCC tissues. **E** Kaplan–Meier survival analysis shows the overall survival rate based on circPRKCA expression. **F** A multivariate Cox regression analysis was conducted to evaluate the prognostic factors associated with ESCC patients. * p < 0.05, ** p < 0.01, *** p < 0.001

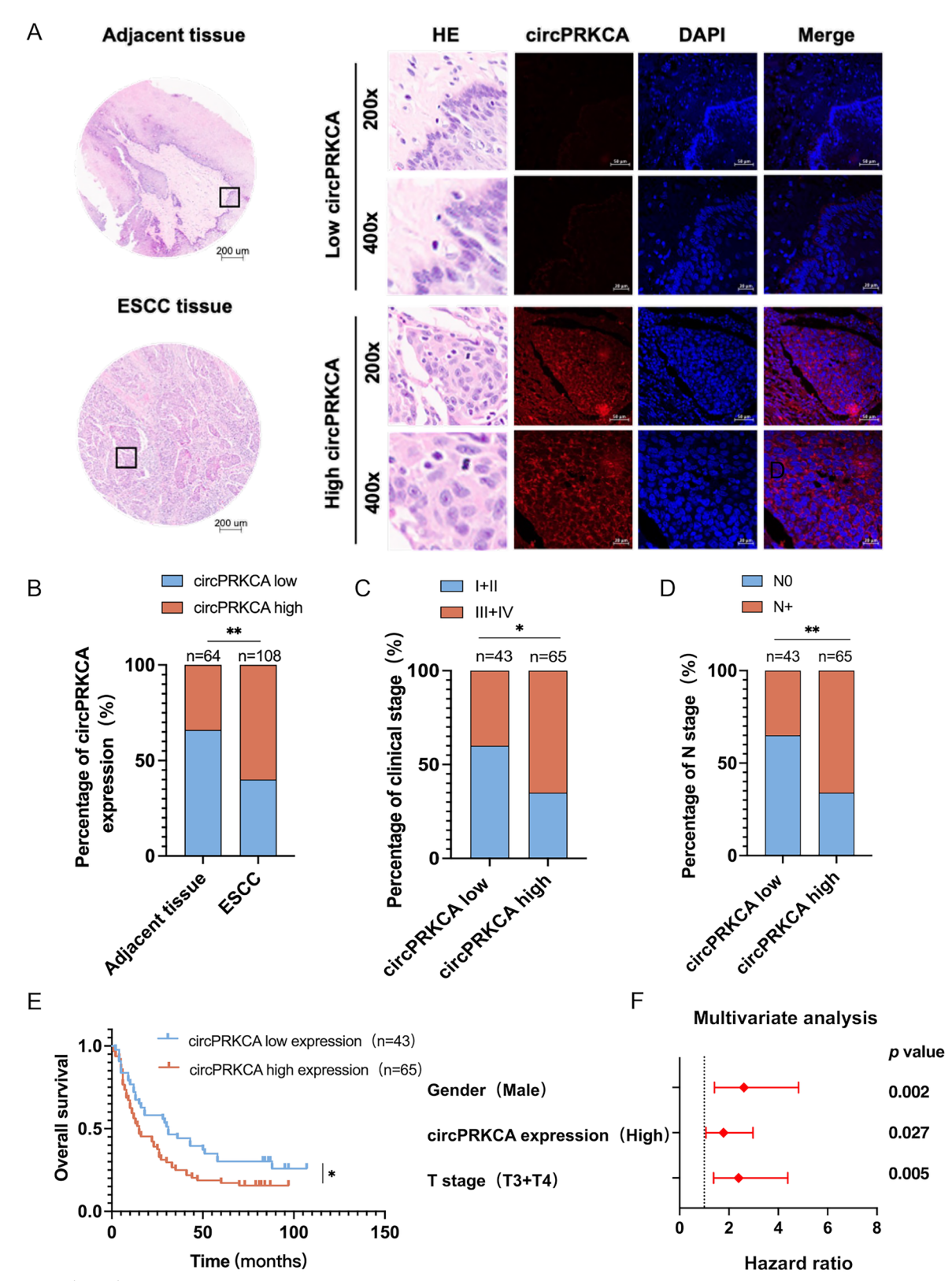


Fig. 2 (See legend on previous page.)

Table 2 Relationship between circPRKCA expression and clinicopathological parameters in ESCC patients

Group	circPRKCA		χ²	р	
	Low	High			
Age			0.040	0.841	
< 60	12	17			
≥60	31	48			
Gender			1.169	0.280	
Male	35	47			
Female	8	18			
T stage			0.137	0.711	
T1 +T2	8	14			
T3+T4	35	51			
N stage			10.178	0.001	
N0	28	22			
N+	15	43			
Pathological stage			1.071	0.301	
I + II	39	53			
III	4	12			
Clinical stage		6.568	0.010		
1+11	26	23			
III + IV	17	42			

RNA. Increasing evidence suggests that circRNAs can exert their functions through interactions with proteins [4, 21]. We conducted two independent RNA pulldown experiments and identified 17 proteins that were enriched in both experiments. Among these, YBX1 captured our attention (Figs. 4B and S3B) due to its strong association with metastasis as an oncogenic protein, a finding corroborated by data from the TCGA database (Fig. 4C). Subsequently, to demonstrate the interaction between circPRKCA and YBX1, Western blot was employed to confirm that the circPRKCA probe could successfully bind to YBX1 (Fig. 4D). RIP and RT-qPCR assays further validated that theYBX1 antibody

could enrich circPRKCA in KYSE30 and KYSE150 cells (Fig. 4E). Additionally, FISH-IF assay revealed the co-localization of circPRKCA and YBX1 in the cytoplasm (Fig. 4F). Next, we investigated the role of YBX1 in promoting circPRKCA-mediated metastasis using scratch healing, transwell migration, matrigel invasion, and tube formation assays. We found that the knockdown of YBX1 in KYSE30 and KYSE150 cells significantly inhibited the migration and invasion capabilities of ESCC cells, as well as the angiogenic potential of HUVEC cells cultured with conditioned medium from ESCC cells. Conversely, the knockdown of YBX1 reversed the promoting effects on these biological functions caused by circPRKCA overexpression (Figs. 4G-I and S3C-E). The results of these rescue experiments indicate that circPRKCA can influence the pro-metastatic phenotype of ESCC by regulating YBX1.

CircPRKCA stabilizes the expression of YBX1 through the ubiquitin (Ub) -proteasome pathway

Next, we explored the specific molecular mechanism linking circPRKCA and YBX1. The knockdown and overexpression of circPRKCA in KYSE30 and KYSE150 cells resulted in decreased and increased levels of YBX1, respectively (Figs. 5A, 5B, S3H, S3I). Notably, this regulatory effect did not significantly alter YBX1 mRNA levels (Fig. S3F, S3G). These findings suggest that circPRKCA influences YBX1 expression at the translational level, warranting a comprehensive investigation into the mechanisms underlying this interaction. We considered whether circPRKCA functions by stabilizing YBX1. To explore this possibility, we conducted CHX (40ug/ml) chase experiments and observed that the knockdown of circPRKCA accelerated YBX1 degradation (Fig. 5C), while the overexpression of circPRKCA promoted YBX1 stability (Fig. 5D). Furthermore, MG132, a ubiquitin-proteasome pathway inhibitor, mitigated the reduction in YBX1

Table 3 Univariate and multivariate analysis of ESCC prognosis

Variable	Univariate analysis			Multivariate analysis		
	p value	HR	95%CI	p value	HR	95%CI
Age (≥60 vs <60)	0.459	1.201	0.740-1.951			
Gender (Male vs Female)	0.002	2.516	1.414-4.479	0.002	2.610	1.413-4.821
circPRKCA expression (High vs low)	0.035	1.615	1.035-2.521	0.027	1.782	1.068-2.975
T stage (T3+T4 vsT1+T2)	0.004	2.402	1.324-4.356	0.005	2.394	1.308-4.383
N stage (N+vs N0)	0.003	1.945	1.255-3.015			
Pathological stage (III vs I+II)	0.538	1.212	0.658-2.232			
Clinical stage (III+IV vs I+II)	< 0.001	2.252	1.443-3.515			

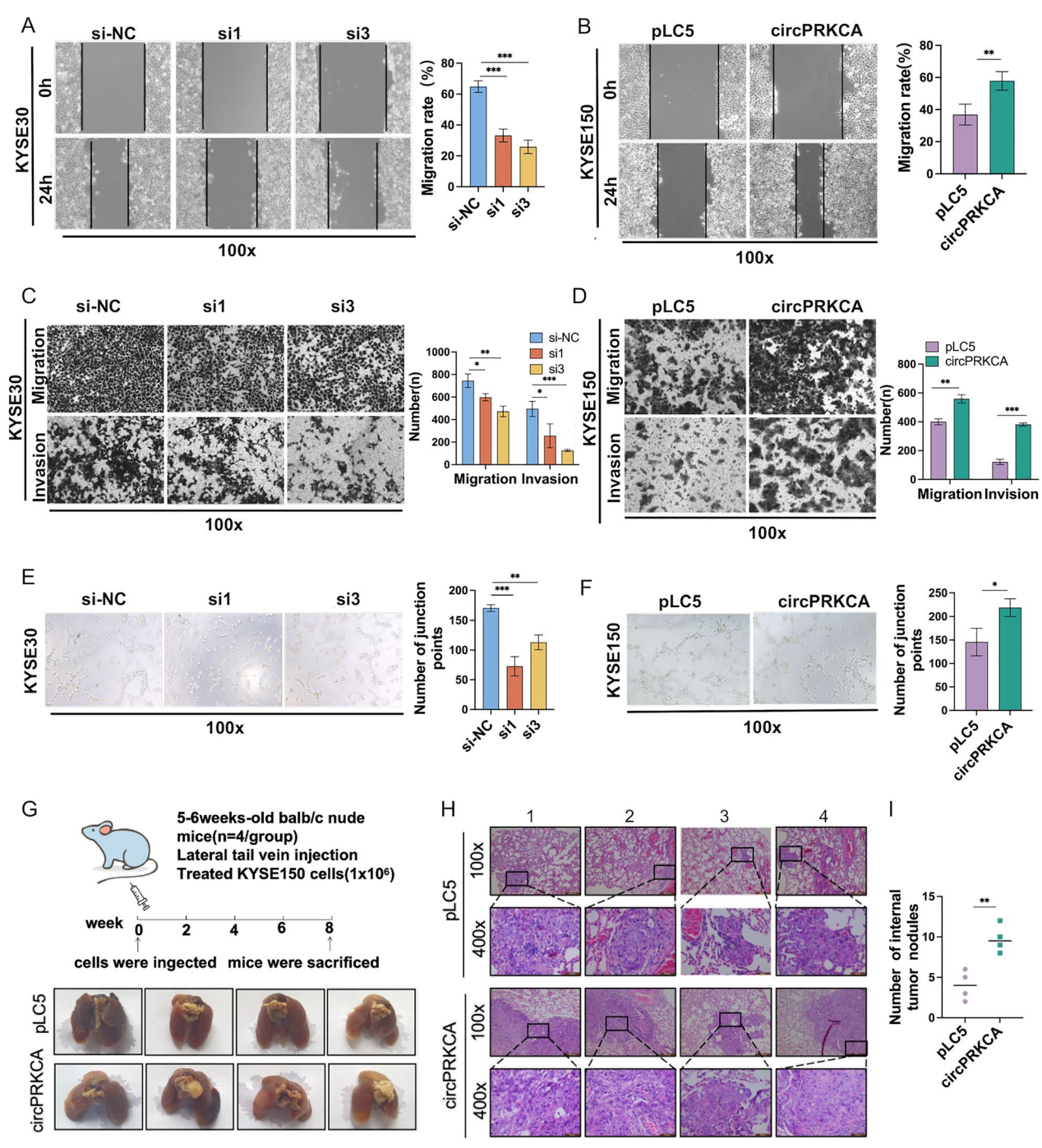


Fig. 3 CircPRKCA facilitates the metastasis of ESCC cells both in vitro and in vivo. **A, B** The scratch healing capacity of ESCC cells transfected with si-circPRKCA, respectively. **C, D** The migration and invasion capabilities of ESCC cells transfected with si-circPRKCA or circPRKCA or circPRKCA, respectively. **E, F** The tube formation assay evaluated the angiogenic potential of HUVEC cells cultured with the conditioned medium from ESCC cells transfected with si-circPRKCA or circPRKCA. **G** A schematic diagram illustrates the construction of a mouse lung metastasis model via the tail vein. **H, I** HE staining assay was performed to observe tumor formation and the number of pulmonary metastases in mice with stable transfection of the pLC5 and circPRKCA groups in KYSE150 cells. * p < 0.005, *** p < 0.001, **** p < 0.001

expression caused by circPRKCA knockdown, and prevented the degradation of YBX1 protein following circPRKCA overexpression. (Fig. 5E, F). Co-IP

verified the endogenous binding of YBX1 to Ub in KYSE30 and KYSE150 cells (Fig. 5G). Additionally, the changes in ubiquitination levels influenced by

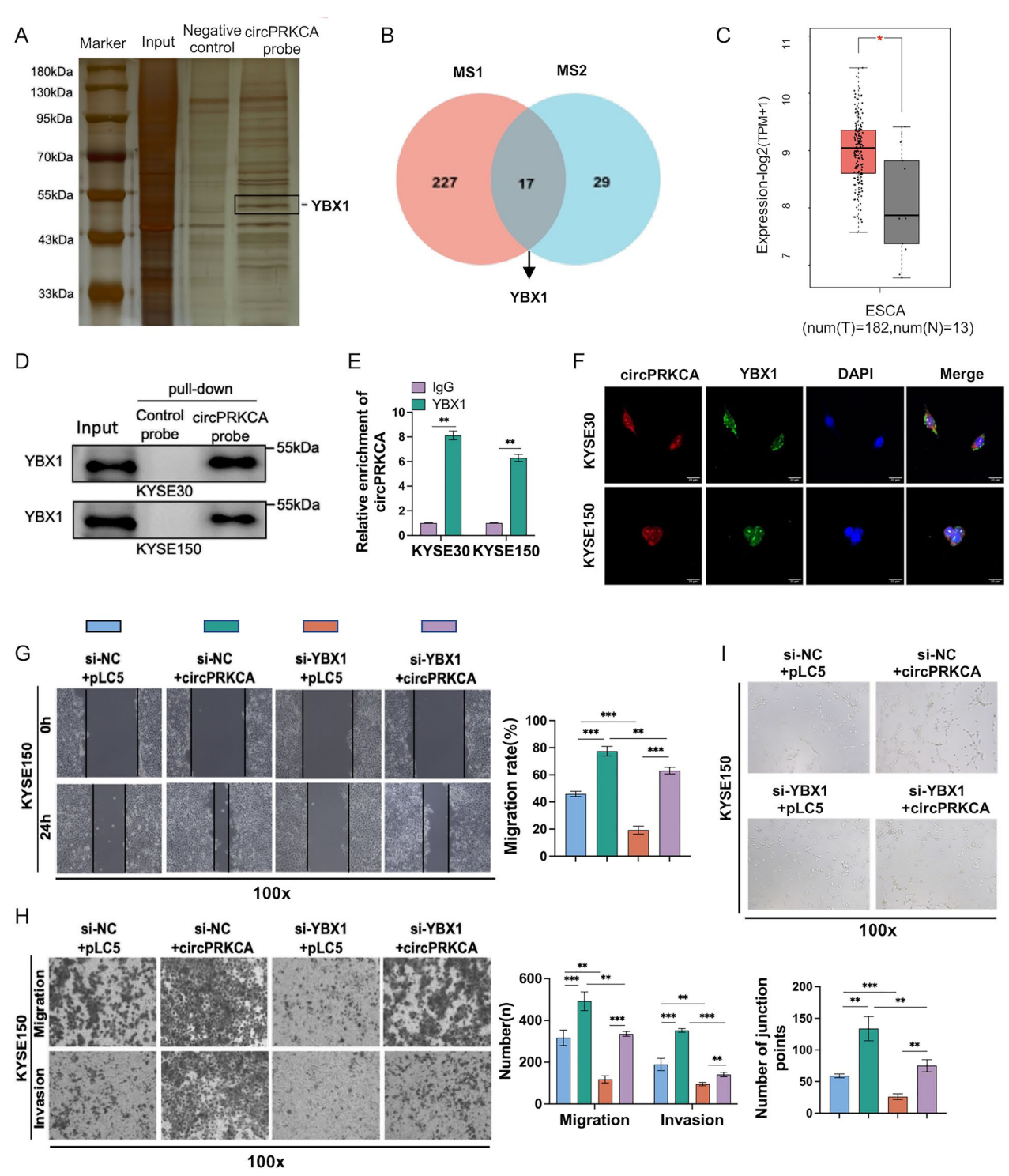


Fig. 4 CircPRKCA binds to YBX1 and promotes ESCC progression. **A** Silver staining representative image of circPRKCA enriched proteins. **B** YBX1 protein was identified in two MS analyses. **C** Validation of the elevated expression of YBX1 in EC using the TCGA database. **D** circPRKCA was shown to interact with YBX1 through western blot analysis. **E** Detection of YBX1 using RIP. **F** Identification of the co-localization of circPRKCA (red) and YBX1 (green) using FISH-IF. **G-I** Rescue experiments confirmed the changes in scratch healing, transwell migration, and matrigel invasion capabilities of KYSE150 cells treated with circPRKCA vector or si-YBX1, as well as the angiogenic potential of HUVEC cells cultured with the supernatant from KYSE150 cells. * p < 0.05, *** p < 0.01, **** p < 0.001, **** p < 0.001

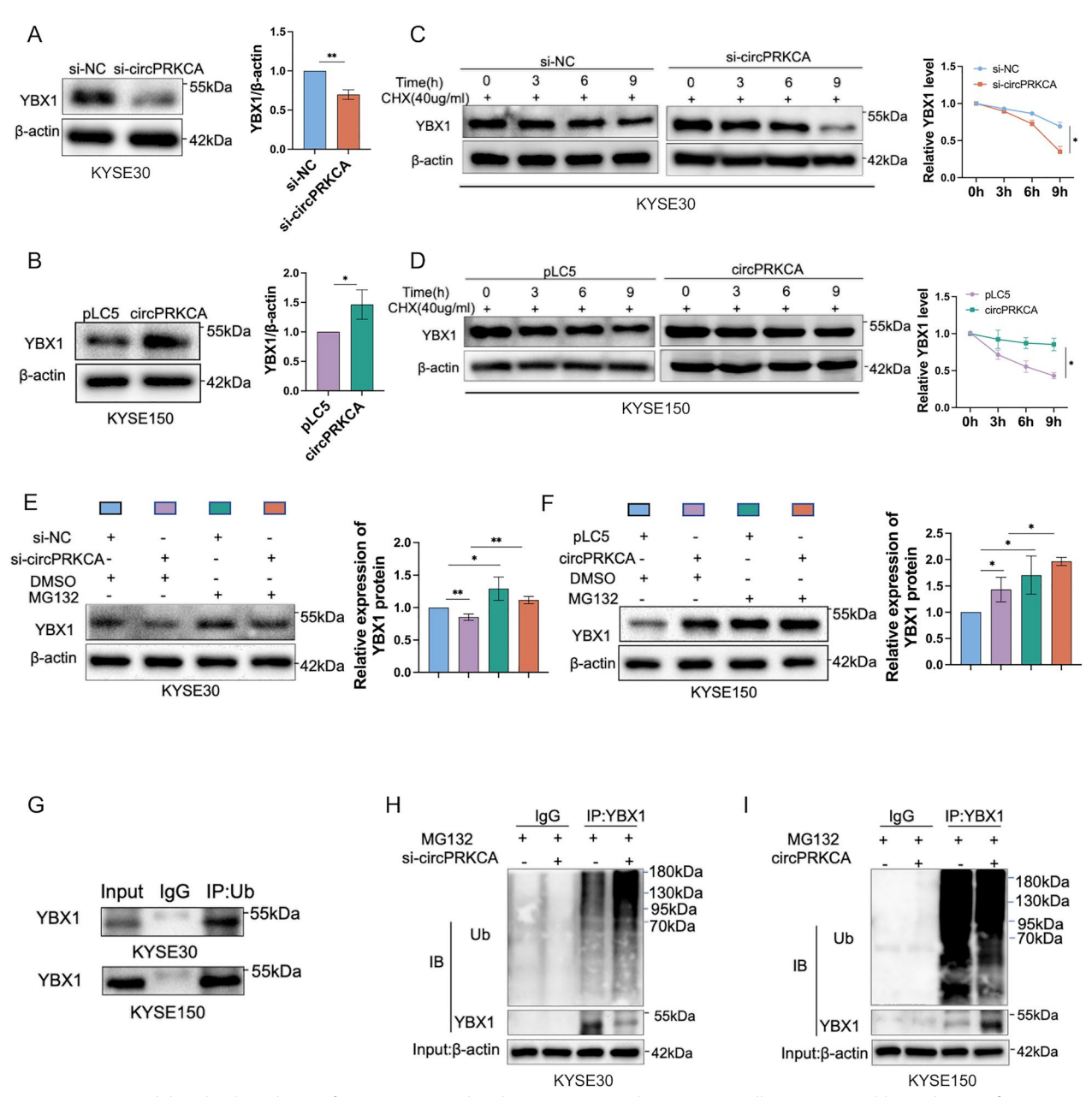


Fig. 5 CircPRKCA inhibits the degradation of YBX1 protein via the Ub–proteasome pathway in ESCC cells. **A, B** Western blot analysis confirms that the knockdown and overexpression of circPRKCA resulted in decreased and increased levels of YBX1, respectively. **C, D** CHX (40 μg/ml) was added to verify that circPRKCA expression can regulate YBX1 degradation. **E, F** Western blot analysis confirms MG132 (20 μM) could reverse the expression of YBX1 regulated by the knockdown or overexpression of circPRKCA. **G** Co-IP method detects the interaction between YBX1 and Ub. **H, I** The Co-IP method reveals that the levels of YBX1 and Ub are regulated by the knockdown or overexpression of circPRKCA. *p < 0.05, **p < 0.01, ***p < 0.001, ***p < 0.001

circPRKCA support these findings, demonstrating that circPRKCA protects YBX1 from degradation by inhibiting the ubiquitin—proteasome pathway (Fig. 5H, I).

CSF2 is a downstream target gene of circPRKCA

In order to elucidate the downstream genes modulated by circPRKCA in ESCC, we performed mRNA sequencing and subsequently analyzed the differentially expressed genes in TE1 cells following the silencing of circPRKCA (Fig. 6A). Based on the screening criteria of p < 0.05 and

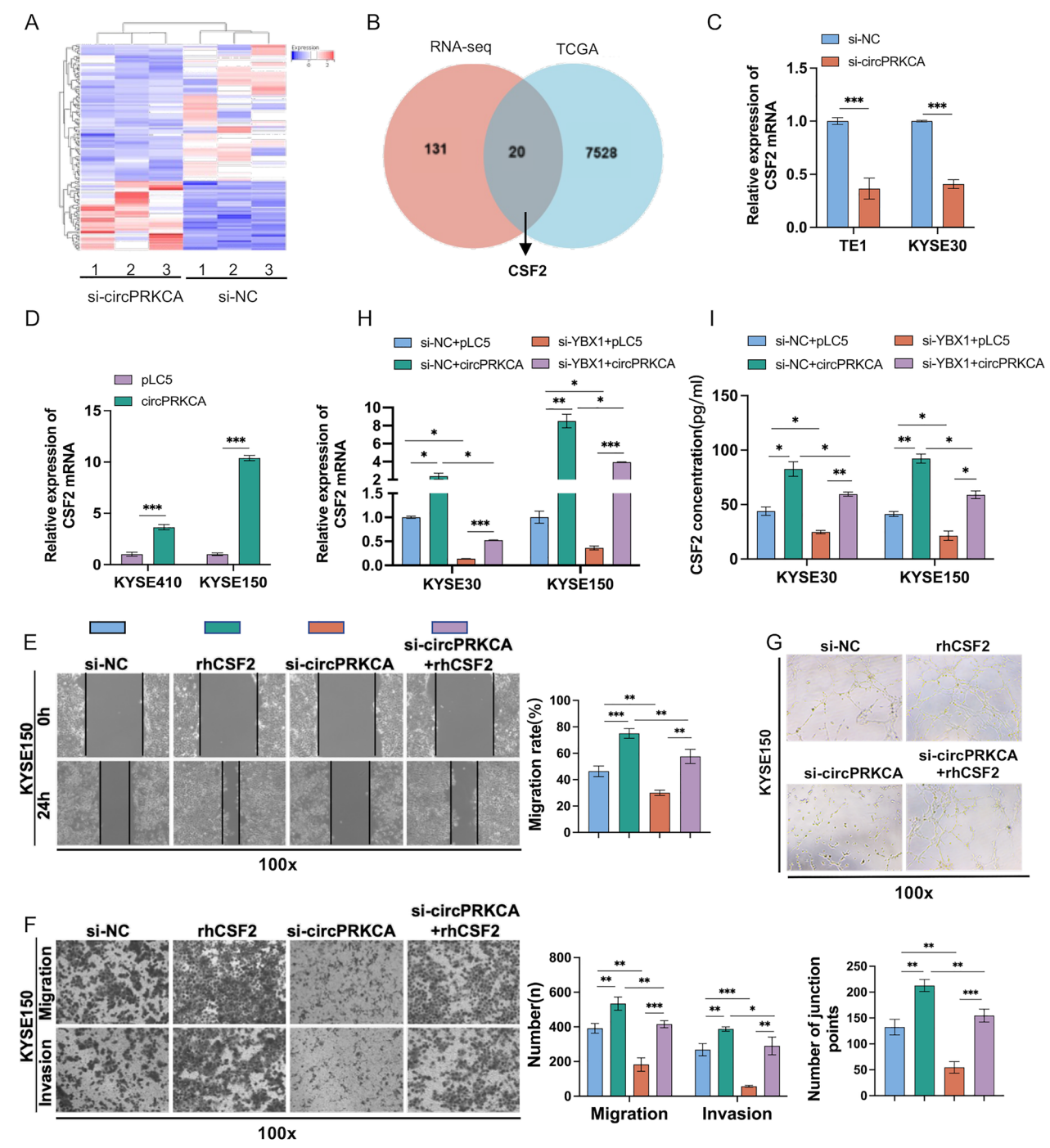


Fig. 6 CSF2 is a downstream gene of circPRKCA in TE1 and KYSE30 cells. **A** Differentially expressed genes in TE1 cells transfected with si-circPRKCA were identified using mRNA sequencing. **B** CSF2 was identified in both the circPRKCA mRNA sequencing dataset and the YBX1-related gene dataset from the TCGA database. **C**, **D** The expression of CSF2 in ESCC cells treated with si-NC/si-circPRKCA and pLC5/circPRKCA were measureed by RT-qPCR. **E-G** Rescue experiments confirmed the changes in scratch healing, transwell migration, and matrigel invasion capabilities of KYSE150 cells under conditions of exogenously added rhCSF2 or the knockdown of circPRKCA, as well as the angiogenic potential of HUVEC cells cultured with medium from KYSE150 cells. **H**, **I** RT-qPCR and ELISA were employed to assess the expression of CSF2 in ESCC cells modulated with circPRKCA or si-YBX1. * p < 0.05, *** p < 0.01, **** p < 0.001

log2|FC|>1, we identified 152 differentially expressed genes. A cross-analysis of these genes with those associated with YBX1 in the TCGA database revealed an overlap of 20 genes (Fig. 6B). Among these, we concentrated on CSF2 due to its notable differential expression and its recognized role as an angiogenic factor implicated in cancer metastasis (Fig. S4A). An examination of the TCGA database reveals that CSF2 is markedly overexpressed in EC and correlates with adverse clinical outcomes (Fig. S4B, S4C). The receiver operating characteristic (ROC) curves indicated that the diagnostic efficiency of CSF2 for EC reached 0.914 (Fig. S4D), suggesting that CSF2 acts as an oncogene in EC. We confirmed the positive regulatory effect of circPRKCA on CSF2 expression using RT-qPCR and ELISA (Fig. 6C, 6D and S4E, S4F). These findings indicate that CSF2 is a downstream gene of circPRKCA.

Subsequently, we further validated the biological functions of CSF2. Rescue experiments confirmed that the exogenous addition of recombinant human CSF2 (rhCSF2) significantly enhances scratch healing, transwell migration, and matrigel invasion capabilities in the KYS150 and KYSE30 cell lines, as well as the angiogenic potential of HUVEC cells co-cultured with conditioned medium from ESCC cells. Notably, rhCSF2 reversed the decreasing effect on these biological functions caused by the knockdown of circPRKCA (Figs. 6E-G and S4G-I). Additionally, analysis of the TCGA database showed that the expression levels of YBX1 and CSF2 were positively correlated. (Fig. S4J). Both RT-qPCR and ELISA confirmed the regulatory effects of the circPRKCA/YBX1 axis on CSF2 at both the transcriptional and translational levels (Fig. 6H, I). These findings prompted us to further investigate the underlying mechanisms by which the circPRKCA/YBX1 axis modulates CSF2 expression.

CircPRKCA/YBX1 regulates the stability of CSF2 mRNA in a manner dependent on m5C modification

YBX1 is an m5C reader. Multiple studies have shown that YBX1 contributes to the stabilization of mRNA by facilitating m5C modification. It remains uncertain whether CSF2 is involved in the m5C modification. RIP assay revealed that YBX1 can bind to CSF2 (Fig. 7A). We also used iRNA-m5C (http://lin-group.cn/server/iRNA-m5C/) and RNAm5Cfinder (http://www.rnanut.net/rnam5cfinder/) databases to search and find multiple potential m5C sites on CSF2. Subsequently, MeRIP analysis was performed to verify that the m5C antibody significantly enriched CSF2 compared to the IgG control group, suggesting that CSF2 can be methylated by m5C (Fig. 7B). Moreover, as we expected, YBX1 knockdown (si2-YBX1 and si3-YBX1) accelerated the degradation of

CSF2 mRNA (Figs. 7C, D and S4K–S4L). To investigate the potential role of circPRKCA in modulating the stability of CSF2 mRNA, possibly mediated by the activity of YBX1, we conducted MeRIP and actinomycin D rescue experiments. Our findings indicate that the knockdown of YBX1 effectively counteracts the increase in binding affinity and mRNA stability that results from the overexpression of circPRKCA (Fig. 7E–H). These results indicated that the circPRKCA/YBX1 complex increased the stabilization of CSF2 mRNA through a mechanism that relies on m5c modifications.

We also examined the expression of YBX1 and CSF2 in metastatic tumors located in the lungs of mice by IHC method. Our results indicated that YBX1 and CSF2 were markedly elevated in the circPRKCA overexpression group in comparison to the pLC5 group (Fig. 7I, J). Additionally, we employed CD31 and CD34 as markers to evaluate angiogenesis within the metastatic nodules, revealing that both CD31 and CD34 was upregulated in the circPRKCA overexpression group. These findings imply that the circPRKCA/YBX1/CSF2 signaling pathway plays a crucial role in facilitating the metastatic progression of ESCC (Fig. 7K).

Discussion

Although traditional treatment modalities, including surgery, radiotherapy, and chemotherapy, have achieved some progress, the prognosis for ESCC patients remains concerning. Distant metastasis continues to be the leading cause of treatment failure in ESCC. Identifying effective therapeutic targets to inhibit metastatic pathways has thus become an urgent priority.

Recent studies suggest that circRNAs hold significant potential as precise therapeutic targets in cancer treatment [22]. However, the specific roles of circRNAs in ESCC remain inadequately understood. In this study, we analyzed 108 ESCC tissue samples and found that circPRKCA is significantly overexpressed in ESCC and is associated with poor survival outcomes. This finding aligns with the growing recognition of circRNAs as potential biomarkers in oncology [23]. Functional assays revealed that circPRKCA enhances the malignant metastatic properties of ESCC cells by promoting migration, invasion, and angiogenesis both in vitro and in vivo. These results are consistent with previous studies demonstrating that circPRKCA drives the progression of non-small cell lung cancer (NSCLC), further highlighting its critical role in regulating tumor cell behavior [24]. Clinically, our findings demonstrate a significant correlation between circPRKCA expression and ESCC patient prognosis. Elevated circPRKCA levels may indicate a higher risk of metastasis, suggesting the need for more aggressive therapeutic strategies. Furthermore, the

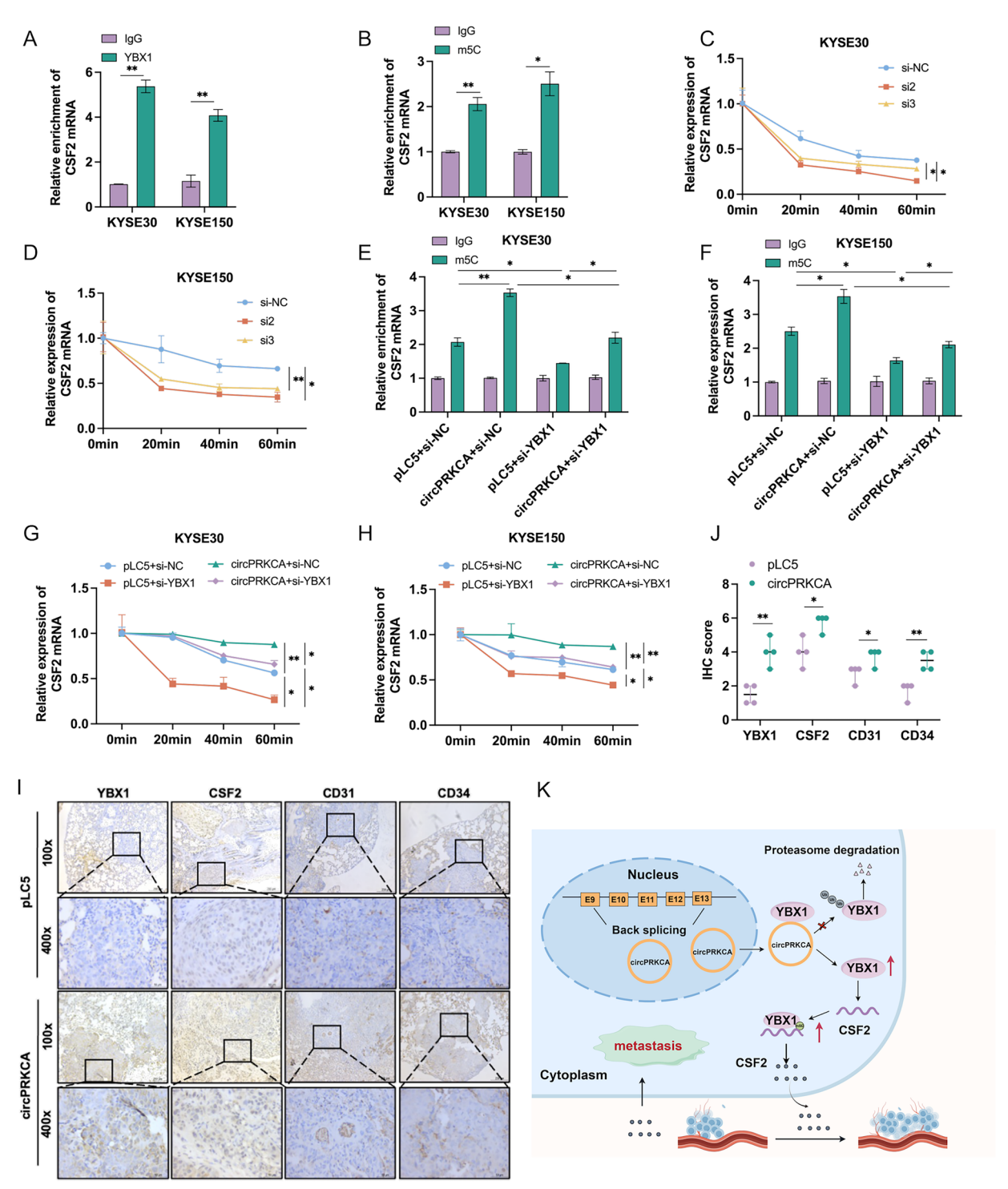


Fig. 7 CircPRKCA/YBX1 enhances the stability of CSF2 mRNA through m5C modification in KYSE30 and KYSE150 cells. **A** RIP assay verifies the interaction between YBX1 and CSF2. **B** MeRIP assay confirms the presence of m5C methylation sites in CSF2. **C, D** Actinomycin D experiments assess the regulation of CSF2 mRNA stability by YBX1. **E, F** A MeRIP experiment verifies the changes in CSF2 mRNA enrichment levels induced by the m5C antibody in ESCC cells transfected with circPRKCA or si-YBX1. **G, H** Salvage experiments confirm the effect of actinomycin D on the stabilization of CSF2 mRNA in ESCC cells regulated by circPRKCA or si-YBX1. **I, J.** The levels of YBX1, CSF2, CD31, and CD34 in the pLC5 and circPRKCA vector groups were detected by IHC. **K** The mechanism of the circPRKCA/YBX1/CSF2 axis in promoting the progression of ESCC metastasis. *p < 0.05, **p < 0.01, ***p < 0.001.

development of targeted therapies against circPRKCA, such as antisense oligonucleotides or siRNA, could provide a promising approach to suppress its expression.

Next, we investigated the mechanism by which circPRKCA promotes ESCC progression through its interaction with RBPs. Our findings demonstrate that circPRKCA regulates YBX1 expression via the Ub-proteasome pathway. Ubiquitination is a well-established post-translational modification, and the Ub-proteasome pathway is recognized as the primary mechanism for protein degradation in eukaryotic cells [25, 26]. By inhibiting YBX1 degradation, circPRKCA upregulates YBX1 levels, thereby promoting ESCC metastasis. This conclusion is supported by CHX chase assay and the use of the proteasome inhibitor MG132, which mitigated the effects of circPRKCA knockdown on YBX1 stability. Currently, research on circRNA-RBP interactions in ESCC metastasis remains limited. Our study highlights a unique mechanism by which circPRKCA interacts with YBX1 via the Ub-proteasome system to drive metastatic progression.

To explore the regulatory role of the circPRKCA/YBX1 axis in gene expression, we performed mRNA sequencing of circPRKCA and overlapped with YBX1 target genes in the TCGA database. Notably, CSF2, a well-known vascular growth factor [27], exhibited the highest fold change in expression. As expected, circPRKCA overexpression upregulated CSF2 expression, while YBX1 knockdown suppressed this effect. Angiogenesis is critical for meeting the increased oxygen and nutrient demands necessary for tumor metastasis [28]. Conditioned medium from circPRKCA-knockdown ESCC cells inhibited angiogenesis in HUVEC cells, whereas the addition of rhCSF2 reversed this effect. These results align with the established role of angiogenesis as a hallmark of cancer progression [29].

Furthermore, the molecular mechanism by which circPRKCA/YBX1 modulates CSF2 has captured our attention. YBX1 has been reported to function as an m5C reader protein, playing a critical role in m5C methylation [30]. The m5C methylation is involved in various cellular processes and has been linked to cancer cell invasion and migration [31–33]. For example, YBX1 stabilizes the m5C-modified ENO1 gene to promote colorectal cancer progression [34]. In our study, a significant positive correlation between YBX1 and CSF2 was observed, and we identified multiple potential m5C binding sites in CSF2 using publicly available databases. These predictions were validated by MeRIP assays, confirming that CSF2 undergoes m5C modification. Additionally, actinomycin

D assays revealed that YBX1 knockdown reduced CSF2 mRNA stability, MeRIP and actinomycin D rescue experiments indicated that the knockdown of YBX1 effectively counteracts the increase in binding affinity and mRNA stability that results from the overexpression of circPRKCA. The results suggest that circPRKCA/YBX1 regulates CSF2 expression in an m5C-dependent manner.

Despite these encouraging results, several limitations should be acknowledged. First, the sample size involved in the clinical analysis is relatively small because of the research condition limitation. Second, this study focuses on the circPRKCA/YBX1/CSF2 signaling pathway, overlooking the possibility that circPRKCA may interact with other RBPs to participate in additional regulatory networks, which warrants further investigation.

In conclusion, this study elucidates a novel mechanism by which circPRKCA regulates the YBX1/CSF2 axis to promote ESCC metastasis and highlights the potential of circPRKCA as a therapeutic target and prognostic biomarker for ESCC (Fig. 7K).

Abbreviations

ESCC Esophageal squamous cell carcinoma

EC Esophageal carcinoma circRNA Circular RNA

RBPs RNA-binding proteins YBX1 Y-box binding protein 1

CSF2 Granulocyte-macrophage colony-stimulating factor

EMT Epithelial-mesenchymal transition

FC The fold change
MeRIP Methylated RNA immunoprecipitation

MeRIP Methylated RNA immunoprecip m5C 5-Methylcytosine FBS Fetal bovine serum

gDNA Genomic DNA cDNA Complementary DNA mRNA Messenger RNA

FISH Fluorescence in situ hybridization

CCK-8 Cell Counting Kit-8

HUVECs Human umbilical vein endothelial cells
ELISA Enzyme-linked immunosorbent assay
FISH-IF FISH-immunofluorescence microscopy

MS Mass spectrometry Co-IP Co-immunoprecipitation ECL Electrochemiluminescence RIP RNA Immunoprecipitation IHC Immunohistochemical DAB Diaminobenzidine Ub Ubiquitin SD Standard deviation H&E Hematoxylin and eosin

ORF Open reading frame
CHX Cycloheximide

ROC Receiver operating characteristic rhCSF2 Recombinant human CSF2 NSCLC Non-small cell lung cancer

Supplementary Information

The online version contains supplementary material available at https://doi.org/10.1186/s12967-025-06395-5.

Supplementary material 1. Fig. S1. The regulation of circPRKCA on the proliferation ability of ESCC cells. (A) Validation of the relative expression levels of circPRKCA in the four ESCC cell lines. (B, C) RT-qPCR was used to confirm the transfection efficiency of the siRNA and overexpression plasmids. (D, G) CCK-8 assay was conducted to evaluate the proliferation capacity of ESCC cells transfected with si-circPRKCA or circPRKCA, respectively. (H, I) Colony formation assay was performed to assess the clonogenic potential of ESCC cells transfected with si-circPRKCA or circPRKCA, respectively. * p < 0.05, **p < 0.01, ***p < 0.001.**

Supplementary material 2. Fig. S2. The effect of circPRKCA expression on the metastatic behavior in ESCC cells. (A, B) The scratch healing ability of ESCC cells regulated by si-circPRKCA or circPRKCA, respectively. (C, D) The migration and invasion capabilities of ESCC cells transfected with si-circPRKCA or circPRKCA, respectively. (E, F) The tube formation assay assessed the angiogenic potential of HUVEC cells cultured with the supernatant from ESCC cells transfected with si-circPRKCA or circPRKCA. (G, H) Fluorescence representative plots of KYSE150 cells stably overexpressing pLC5 and circPRKCA, along with the assessment of overexpression efficiency using RT-qPCR. * p < 0.05, ** p < 0.01, *** p < 0.001.

Supplementary material 3. Fig. S3. CircPRKCA binds to YBX1 and promotes the aggressive progression of ESCC. (A) Representative silver-stained image of the RNA pull-down assay. (B) Specific peptide segments of the YBX1 protein. (C-E) Rescue experiments confirmed the effects of circPRKCA overexpression and YBX1 knockdown on scratch healing, transwell migration, and matrigel invasion capabilities of KYSE30 cells, along with the angiogenic potential of HUVEC cells cultured with medium from KYSE30 cells. (F, G) RT-qPCR was employed to validate the regulatory effect of circPRKCA on YBX1 mRNA levels. (H, I) In TE1 and KYSE410 cells, western blot verified the relationship between circPRKCA knockdown or overexpression and YBX1, respectively. * p < 0.05, ** p < 0.01, *** p < 0.001.

Supplementary material 4. Fig. S4. CircPRKCA facilitates the progression of ESCC cells by modulating CSF2. (A) Heatmap of downstream target genes derived from RNA-seq analysis. (B) The high expression levels of CSF2 in EC was analysed in TCGA database. (C) The Kaplan-Meier curve indicates that CSF2 is associated with worse prognosis in EC. (D) The ROC curve suggests that CSF2 exhibits high diagnostic efficacy for EC. (E, F) CSF2 was regulated by si-NC/si-circPRKCA and pLC5/circPRKCA in ESCC cells, as measured using ELISA. (G-I) Rescue experiments confirmed the alterations in scratch healing, transwell migration, and matrigel invasion capabilities of KYSE30 cells under conditions of exogenously added rhCSF2 or the knockdown of circPRKCA, as well as the angiogenic potential of HUVEC cells cultured with medium from KYSE30 cells. (J) An examination of the positive relationship between YBX1 and CSF2 in the TCGA database. (K, L) The effectiveness of siRNA aimed at YBX1 was confirmed through RT-qPCR and western blot analysis. * p < 0.05, ** p < 0.01, *** p < 0.001.

Acknowledgements

Not applicable.

Author contributions

Lixia Wu and Lina Gu: Experimental manipulation and completion of the first draft. Yangzheng and jingjing Liu: Data collation and analysis. Zishuan Wei and Fei Liu: prepared all the figures; Lingjiao Meng and Meixiang Sang: Methodology and validation. Jiali Li and Yang Sang: Animal experiment; Lianmei Zhao: Experimental design, Project administration, Resources, Supervision, Writing-review & editing. Baoen Shan: Funding acquisition, Project administration, Writing-review & editing.

Funding

This work was supported by grants from the National Natural Science Foundation of China (Grant No. U21A20415), the Hebei Natural Science Foundation (H2022206525).

Availability of data and materials

The datasets supporting the conclusions of this article are included within the article and its additional files

Declarations

Ethics approval and consent to participate

Informed consent was obtained from all individuals participating in the study (SHYJS-CP-2004003). Animal studies were approved by the Institutional Animal Care and Use Committee of Fourth Hospital of Hebei Medical University (IACUC-4th Hos Hebmu-2023223).

Competing interests

The authors have declared that no competing interest exists.

Author details

¹Research Center, The Fourth Hospital of Hebei Medical University, Shijiazhuang 050011, Hebei, China. ²Key Laboratory of Tumor Prevention and Precision Diagnosis and Treatment of Hebei, Clinical Oncology Research Center, The Fourth Hospital of Hebei Medical University, Jiankang Road 12, Shijiazhuang 050011, Hebei, China. ³Animal Care and Use Committee of the Fourth Affiliated Hospital of Hebei Medical University, Shijiazhuang 050011, Hebei, China. ⁴Shanghai Electric Power Hospital, Shanghai 200050, China.

Received: 9 December 2024 Accepted: 18 March 2025 Published online: 01 April 2025

References

- Yang H, Wang F, Hallemeier CL, Lerut T, Fu J. Oesophageal cancer. Lancet. 2024;404(10466):1991–2005.
- Zhu J, Du L, Li H, Ran X, Zeng H, Wei W. Clinicopathological and therapeutic comparisons of esophageal cancer between China and the USA: a multicenter hospital-based study. J Natl Cancer Cent. 2024;4(4):318–25.
- Jiang G, Wang Z, Cheng Z, Wang W, Lu S, Zhang Z, et al. The integrated molecular and histological analysis defines subtypes of esophageal squamous cell carcinoma. Nat Commun. 2024;15(1):8988.
- Yu X, Tong H, Chen J, Tang C, Wang S, Si Y, et al. CircRNA MBOAT2 promotes intrahepatic cholangiocarcinoma progression and lipid metabolism reprogramming by stabilizing PTBP1 to facilitate FASN mRNA cytoplasmic export. Cell Death Dis. 2023;14(1):20.
- Chen W, Xu J, Wu Y, Liang B, Yan M, Sun C, et al. The potential role and mechanism of circRNA/miRNA axis in cholesterol synthesis. Int J Biol Sci. 2023;19(9):2879–96.
- Cao SQ, Xue ST, Li WJ, Hu GS, Wu ZG, Zheng JC, et al. CircHIPK3 regulates fatty acid metabolism through miR-637/FASN axis to promote esophageal squamous cell carcinoma. Cell Death Discov. 2024;10(1):110.
- Zhang X, Bian Y, Li Q, Yu C, Gao Y, Tian B, et al. EIF4A3-mediated oncogenic circRNA hsa_circ_0001165 advances esophageal squamous cell carcinoma progression through the miR-381-3p/TNS3 pathway. Cell Biol Toxicol. 2024;40(1):84.
- Hu X, Chen G, Huang Y, Cheng Q, Zhuo J, Su R, et al. Integrated multiomics reveals silencing of has_circ_0006646 promotes TRIM21-mediated NCL ubiquitination to inhibit hepatocellular carcinoma metastasis. Adv Sci. 2024;11(16): e2306915.
- Li R, Wang J, Xie Z, Tian X, Hou J, Wang D, et al. CircUSP1 as a novel marker promotes gastric cancer progression via stabilizing HuR to upregulate USP1 and Vimentin. Oncogene. 2024;43(14):1033–49.
- Gu L, Sang Y, Nan X, Zheng Y, Liu F, Meng L, et al. circCYP24A1 facilitates esophageal squamous cell carcinoma progression through binding PKM2 to regulate NF-κB-induced CCL5 secretion. Mol Cancer. 2022;21(1):217.
- Sun T, Zhang P, Zhang Q, Wang B, Zhao Q, Liu F, et al. Transcriptome analysis reveals PRKCA as a potential therapeutic target for overcoming cisplatin resistance in lung cancer through ferroptosis. Heliyon. 2024;10(10): e30780.
- Dinh NTM, Nguyen TM, Park MK, Lee CH. Y-box binding protein 1: unraveling the multifaceted role in cancer development and therapeutic potential. Int J Mol Sci. 2024;25(2):717.

- Wang Y, Wei J, Feng L, Li O, Huang L, Zhou S, et al. Aberrant m5C hypermethylation mediates intrinsic resistance to gefitinib through NSUN2/ YBX1/QSOX1 axis in EGFR-mutant non-small-cell lung cancer. Mol Cancer. 2023;22(1):81.
- Lin C, Lin P, Yao H, Liu S, Lin X, He R, et al. Modulation of YBX1-mediated PANoptosis inhibition by PPM1B and USP10 confers chemoresistance to oxaliplatin in gastric cancer. Cancer Lett. 2024;587: 216712.
- Huang HW, Chen CY, Huang YH, Yeh CT, Wang CS, Chang CC, et al. CMAHP promotes metastasis by reducing ubiquitination of Snail and inducing angiogenesis via GM-CSF overexpression in gastric cancer. Oncogene. 2022;41(2):159–72.
- Yu X, Li S, Ke S, Ye C, Wang Q, Wang H, et al. CSF2 impairs Nrf2 signaling through the Akt/Mtor pathway in the development of bladder cancer. J Cancer. 2024;15(11):3242–53.
- Yonemitsu K, Pan C, Fujiwara Y, Miyasato Y, Shiota T, Yano H, et al. GM-CSF derived from the inflammatory microenvironment potentially enhanced PD-L1 expression on tumor-associated macrophages in human breast cancer. Sci Rep. 2022;12(1):12007.
- Ding P, Wu H, Wu J, Li T, He J, Ju Y, et al. N6-methyladenosine modified circPAK2 promotes lymph node metastasis via targeting IGF2BPs/VEGFA signaling in gastric cancer. Oncogene. 2024;43(34):2548–63.
- Liu J, Wei Z, Meng L, Wu L, Liu F, Sang M, et al. CircJPH1 regulates the NF-κB/HERC5 axis to promote the malignant progression of esophageal squamous cell carcinoma through binding to XRCC6. Cell Signal. 2024;124: 111403.
- Zhang Y, Du P, Li Y, Zhu Q, Song X, Liu S, et al. TASP1 promotes gallbladder cancer cell proliferation and metastasis by Up-regulating FAM49B via PI3K/AKT pathway. Int J Biol Sci. 2020;16(5):739–51.
- Yang F, Ma Q, Huang B, Wang X, Pan X, Yu T, et al. CircNFATC3 promotes the proliferation of gastric cancer through binding to IGF2BP3 and restricting its ubiquitination to enhance CCND1 mRNA stability. J Transl Med. 2023;21(1):402.
- Shoda K, Kuwano Y, Ichikawa D, Masuda K. circRNA: a new biomarker and therapeutic target for esophageal cancer. Biomedicines. 2022;10(7):10.
- Kristensen LS, Jakobsen T, Hager H, Kjems J. The emerging roles of circR-NAs in cancer and oncology. Nat Rev Clin Oncol. 2022;19(3):188–206.
- Xu X, Zhang X, Zhang Y, Wang Z. Curcumin suppresses the malignancy of non-small cell lung cancer by modulating the circ-PRKCA/miR-384/ITGB1 pathway. Biomed Pharmacother. 2021;138: 111439.
- Gao L, Zhang W, Shi XH, Chang X, Han Y, Liu C, et al. The mechanism of linear ubiquitination in regulating cell death and correlative diseases. Cell Death Dis. 2023;14(10):659.
- Sun L, Chen Y, Xia L, Wang J, Zhu J, Li J, et al. TRIM69 suppressed the anoikis resistance and metastasis of gastric cancer through ubiquitin-proteasome-mediated degradation of PRKCD. Oncogene. 2023;42(49):3619–32.
- Lopes-Santos G, Tjioe KC, Magalhaes MAO, Oliveira DT. The role of granulocyte-macrophage colony-stimulating factor in head and neck cancer. Arch Oral Biol. 2023;147: 105641.
- Yang M, Mu Y, Yu X, Gao D, Zhang W, Li Y, et al. Survival strategies: How tumor hypoxia microenvironment orchestrates angiogenesis. Biomed Pharmacother. 2024;176: 116783.
- Guelfi S, Hodivala-Dilke K, Bergers G. Targeting the tumour vasculature: from vessel destruction to promotion. Nat Rev Cancer. 2024;24(10):655–75.
- Liu K, Xu P, Lv J, Ge H, Yan Z, Huang S, et al. Peritoneal high-fat environment promotes peritoneal metastasis of gastric cancer cells through activation of NSUN2-mediated ORAI2 m5C modification. Oncogene. 2023;42(24):1980–93.
- 31. Tang Q, Li L, Wang Y, Wu P, Hou X, Ouyang J, et al. RNA modifications in cancer. Br J Cancer. 2023;129(2):204–21.
- Haruehanroengra P, Zheng YY, Zhou Y, Huang Y, Sheng J. RNA modifications and cancer. RNA Biol. 2020;17(11):1560–75.
- 33. Barbieri I, Kouzarides T. Role of RNA modifications in cancer. Nat Rev Cancer. 2020;20(6):303–22.
- 34. Chen B, Deng Y, Hong Y, Fan L, Zhai X, Hu H, et al. Metabolic recoding of NSUN2-mediated m(5)c modification promotes the progression of colorectal cancer via the NSUN2/YBX1/m(5)C-ENO1 positive feedback loop. Adv Sci (Weinh). 2024;11(28): e2309840.

Publisher's Note

Springer Nature remains neutral with regard to jurisdictional claims in published maps and institutional affiliations.